

## Experimental Evidence of Nonlinear Focusing in Standing Water Waves

Yuchen He<sup>1,\*</sup>, Alexey Slunyaev<sup>2,3</sup>, Nobuhito Mori<sup>4</sup>, and Amin Chabchoub<sup>5,4,1,†</sup>

<sup>1</sup>Centre for Wind, Waves and Water, School of Civil Engineering, The University of Sydney, Sydney, NSW 2006, Australia

<sup>2</sup>National Research University-Higher School of Economics, 25 Bol'shaya Pechorskaya Street, Nizhny Novgorod 603950, Russia

<sup>3</sup>Institute of Applied Physics RAS, 46 Ulyanova Street, Nizhny Novgorod 603950, Russia

<sup>4</sup>Disaster Prevention Research Institute, Kyoto University, Uji, Kyoto 611-0011, Japan

<sup>5</sup>Hakubi Center for Advanced Research, Kyoto University, Yoshida-Honmachi, Kyoto 606-8501, Japan



(Received 4 February 2022; accepted 17 August 2022; published 28 September 2022)

Nonlinear wave focusing originating from the universal modulation instability (MI) is responsible for the formation of strong wave localizations on the water surface and in nonlinear wave guides, such as optical Kerr media and plasma. Such extreme wave dynamics can be described by breather solutions of the nonlinear Schrödinger equation (NLSE) like by way of example the famed doubly-localized Peregrine breathers (PB), which typify particular cases of MI. On the other hand, it has been suggested that the MI relevance weakens when the wave field becomes broadband or directional. Here, we provide experimental evidence of nonlinear and distinct PB-type focusing in standing water waves describing the scenario of two counterpropagating wave trains. The collected collinear wave measurements are in excellent agreement with the hydrodynamic coupled NLSE (CNLSE) and suggest that MI can undisturbedly prevail during the interplay of several wave systems and emphasize the potential role of exact NLSE solutions in extreme wave formation beyond the formal narrow band and unidirectional limits. Our work may inspire further experimental investigations in various nonlinear wave guides governed by CNLSE frameworks as well as theoretical progress to predict strong wave coherence in directional fields.

DOI: [10.1103/PhysRevLett.129.144502](https://doi.org/10.1103/PhysRevLett.129.144502)

The emergence of strongly localized waves in nonlinear dispersive media is an actively investigated field of research across wave physics [1–5]. While excluding any external effects on a wave system, extreme wave formations in unidirectional wave guides can be explained either as a result of unstable nonlinear wave interaction [6,7], or the linear superposition principle [8,9]. Both mechanisms have been intensively studied in laboratory environments and the ocean [10,11]. The modulation instability (MI) is a nonlinear wave focusing mechanism [12,13], which has been proven to be present in complex sea states, such as crossing seas [14–16], however being less dominant compared with wave systems with a single wave vector due to the violation of both critical assumptions, namely unidirectionality and narrow band energy level [17,18].

Then again, it has been recently conjectured that there is an increase of probability of rogue wave formation in coupled two-wave systems compared with an uncoupled directional wave field [19]. A coupled nonlinear Schrödinger (CNLSE) framework was already derived for water waves in the '80s [20] and is nowadays considered a fundamental dynamical system for the study of complex, coherent, directional, and rogue wave dynamics in various physical media [21–25].

In this Letter, we provide experimental evidence of nonlinear wave focusing in standing wave fields using the Peregrine breather (PB) [26] as a referenced nonlinear

rogue wave and special MI model evolving in one of two counter-propagating wave systems. It is shown that Peregrine-type unsteady packets on finite and zero background can distinctly evolve in the presence of a counter-propagative regular wave field without any noticeable disturbance nor disintegration of coherence during wave focusing and defocusing. The experimental results are in excellent agreement with the hydrodynamic CNLSE. Moreover, we can confirm nonlinear focusing in such simplified but representative configuration by means of direct numerical simulations of the governing water wave equations using the high-order spectral method (HOSM) for potential flows.

The nonlinear interaction of standing waves involving an incident wave field characterized by the complex amplitude  $\psi^{(1)}(x, t)$  with wave number  $\kappa^{(1)} = (k, 0)$  interacting with the reflected waves  $\psi^{(2)}(x, t)$  with wave number  $\kappa^{(2)} = (-k, 0)$ , and propagating along the space coordinate  $x$ , can be described by the CNLSE [20,21]

$$\begin{aligned}
 i \left( \psi_x^{(1)} + \frac{1}{c_g} \psi_t^{(1)} \right) + \delta \psi_{tt}^{(1)} + \nu (|\psi^{(1)}|^2 - 2|\psi^{(2)}|^2) \psi^{(1)} &= 0 \\
 i \left( \psi_x^{(2)} - \frac{1}{c_g} \psi_t^{(2)} \right) + \delta \psi_{tt}^{(2)} + \nu (|\psi^{(2)}|^2 - 2|\psi^{(1)}|^2) \psi^{(2)} &= 0.
 \end{aligned}
 \tag{1}$$

The angular frequency  $\omega^{(i)}$  and wave number  $\kappa^{(i)}$  are connected through the deep-water linear dispersion relation  $\omega^{(i)} = \sqrt{g|\kappa^{(i)}|}$ ,  $i = 1, 2$  with  $g$  being the gravitational acceleration, while the CNLSE parameters read as

$$c_g = \frac{\omega}{2k}, \quad \delta = -\frac{k}{\omega^2}, \quad \nu = -k^3. \quad (2)$$

The standing water surface elevation describing the interaction between the incident wave field  $\psi^{(1)}$  and opposing wave system  $\psi^{(2)}$  to the first order of approximation is calculated by means of the complex envelope following the expression

$$\eta(x, t) = \frac{1}{2}(\psi^{(1)}(x, t) \exp[i(kx - \omega t)] + \psi^{(2)}(x, t) \exp[-i(kx + \omega t)] + \text{c.c.}). \quad (3)$$

Here, c.c. denotes the complex conjugation, and we emphasize the weakening of the bound wave contributions in standing wave systems in contrast to the unidirectional wave evolution. Our wave modeling will be restricted to the CNLSE, described by the set of equations in Eq. (1); nonetheless, we would like to also highlight that a higher- and fourth-order CNLSE can be applied to two wave systems with different wave frequencies or directions [27].

We investigate the possibility of nonlinear wave focusing in a standing wave field, which is a special case of crossing wave systems with a crossing angle of  $\pi$ , by using the PB model as an incident wave field  $\psi^{(1)}$  and a regular wave envelope of the same amplitude for  $\psi^{(2)}$ . We recall that the PB is a doubly localized solution of the unidirectional nonlinear Schrödinger equation (NLSE) [26], which has been so far observed in optics, water waves, and plasma [28–30]. That said, this solution describes the nonlinear stage of modulation instability in the case of infinitely long perturbation [31,32] and has a rational growth. In fact, it can be approached by either Akhmediev [33,34] or Kuznetsov breathers [35], and so far has not been discussed in the context of collinear waves. Its counterpart on zero background is also known as the degenerate soliton [36].

Since most of the state of the art wave flumes do not have two wave generators on opposing sides, one possibility to allow for wave train collisions is to make use of the wall at the opposite side of the wave generator as a reflective mirror for long-crested waves [37]. Indeed, the absence of wave energy absorbing beach in a perfectly aligned flume permits a full reflection and thus, the formation of standing waves. Such an adjusted and adopted set-up configuration can be viewed in Fig. 1.

The facility operates a piston-type wave paddle to generate boundary conditions in a form of surface elevation time series. The tank has the dimensions  $30 \times 1 \times 1 \text{ m}^3$ , the water depth is set to be 0.75 m, and eight resistive wave

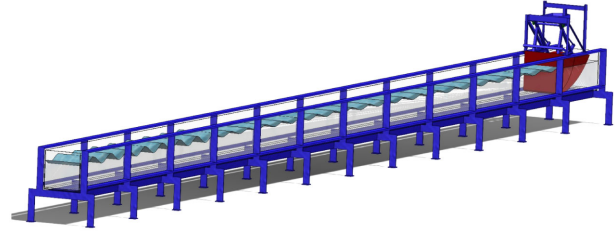


FIG. 1. Sketch of the wave flume setup as installed at the University of Sydney after removing the artificial beach installation to enable full wave reflection. The piston-type wave generator on the right end generates long-crested unidirectional waves. The glass wall at the opposing end acts as a wave reflector.

gauges with a sampling rate of 32 Hz are used to measure the water surface elevation. The accurate controlled generation of the wave field allows the reiteration of the experiments with different wave gauge placements to ensure a high resolution also along the waves' propagation direction [4].

Since we are interested in the interaction of an incident PB wave field with a regular wave train with opposing wave vector, a dynamic head-on interaction which we will refer to as standing PB, we simply select a sufficiently long realization of the PB solution in time to guarantee the propagation of the unperturbed regular wave to the wall and back, before the wave paddle launches the small and localized Peregrine-specific modulation. We refer to Refs. [29,38] for the construction of the dimensional Peregrine boundary conditions. In our experiments we chose the amplitude to be  $a = 0.01 \text{ m}$  for two carrier steepness values  $ak = 0.09$  and  $ak = 0.10$ , which corresponds to a difference in wavelength of 0.07 m. The respective values of the wave frequency can be computed using the linear dispersion relation  $\omega = \sqrt{gk}$ . Note that the steepness values of  $ak = 0.10$  represent the experimental threshold value before the onset of wave breaking, as observed in our facility. Because of the limited length of our wave flume, considerably reducing the value of wave steepness would not allow us to start our experiments from a small amplitude modulation of the unstable incident wave field. The boundary conditions have been defined to expect the maximal wave compression to be 16 m from the wave generator. The results of the experimental campaign, accounting for 184 measurements along the longitudinal direction for each realization, together with the associated CNLSE predictions, are shown in Fig. 2.

The numerical CNLSE simulations have been carried out for the same wave parameters and boundary conditions as the laboratory experiments for validations purposes. A pseudospectral approach and the fourth-order Runge-Kutta method have been adopted for the integration in space.

The wave tank measurements show an excellent agreement with the CNLSE dynamics: the PB remarkably evolves in standing wave states without any signs of

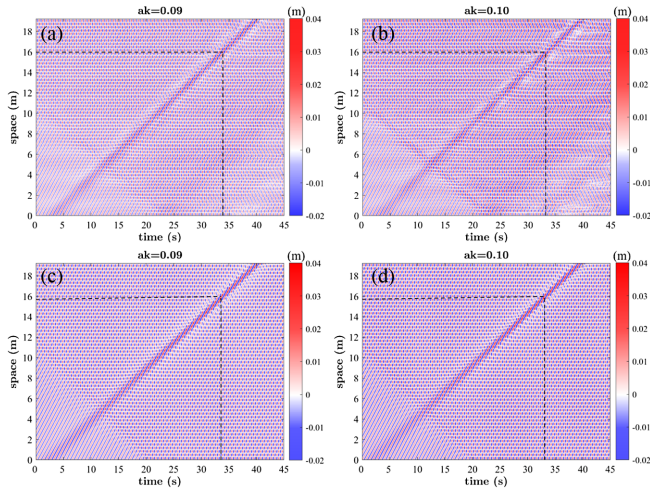


FIG. 2. Top (a) and (b) Experimental observation of two standing PBs as measured by the wave gauges. Bottom (c) and (d) Results of numerical CNLSE simulations starting from the same boundary conditions as the laboratory experiments. Left (a) and (c) Wave parameters  $a = 0.01$  m and  $ak = 0.09$ . Right (b) and (d) Wave parameters  $a = 0.01$  m and  $ak = 0.10$ .

disintegration while keeping its coherence. A video showing this intriguing hydrodynamics is provided in the Supplemental Material [39]. Moreover, the characteristic amplitude amplification of four in this collinear case is also reached at the expected location in the water wave tank. This wave interaction can be also confirmed when studying the respective bispectral evolution; see Fig. 3.

Here, the decomposition of incident and reflected wave constituents in the bispectra, which are estimated from the Fourier components [40], prove that the extreme wave focusing only occurs for incident waves, dominated by the PB dynamics. To be more precise, the spectral broadening, which is an indicator of physical wave focusing, occurs only in the incident wave field, as in Figs. 3(c) and 3(d). On the other hand, the energy of the counterpropagating waves remains steady; see Figs. 3(e) and 3(f). We can also notice that the second harmonic energy weakens when the standing wave field has been fully developed.

Note that the variations in surface wave profiles are very sensitive to the single gauge location. On a node point, the amplitude of the standing regular wave field is zero [41]. It is also worth mentioning that the PB did not have any influence in the destabilization of the regular opposing wave field. This persistence may be partly explained by the form of the CNLSE [Eq. (1)], which supports conservation of integrals  $\int_{-\infty}^{\infty} |\psi_j|^2 dt$  for  $j = 1, 2$ , so that the nonlinear exchange terms in Eq. (1) lead to wavenumber corrections only. The impossibility of energy exchange between two counterpropagating planar deep-water wave systems due to nonlinear four-wave interactions beyond the narrow band approximation was recently emphasized [42,43]. Nonetheless, the generation of collinear opposite waves was observed in fully nonlinear hydrodynamic simulations in Ref. [44].

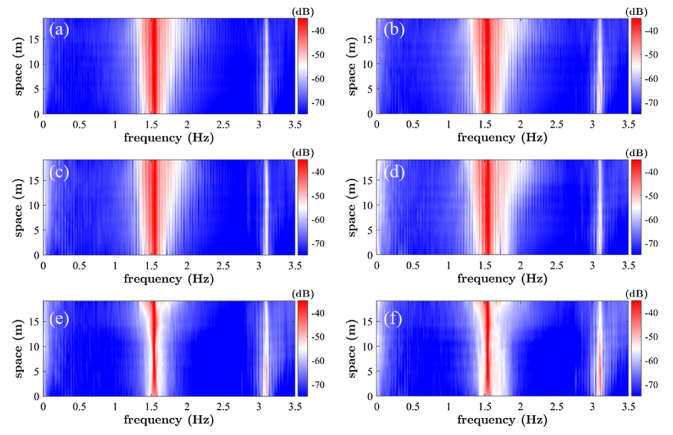


FIG. 3. Spectral evolution of the standing Peregrine breathers, reported in Fig. 2. (a) Computed for the measured surface elevation for the carrier parameters  $a = 0.01$  m and  $ak = 0.09$ . (c) Incident PB wave dynamics isolated from (a). (e) Opposing wave train as isolated from (a). (b) Computed for the measured surface elevation for the carrier wave parameters  $a = 0.01$  m and  $ak = 0.10$ . (d) Incident PB wave dynamics isolated from (b). (f) Opposing wave train as isolated from (b).

In the following we investigate the evolution of the PB counterpart on zero background [36,45], i.e., the degenerate soliton solution, in the presence of a counterpropagative regular wave field. Because this particular NLSE solution has finite length construction on a zero background, the standing wave patterns appear only locally during the interaction with the opposing wave field. Experimental data and respective CNLSE simulations are displayed in Fig. 4.

Since we do have a sufficiently good resolution in the space of  $dx = 0.11$  m, we can reconstruct the spatial profile from the measured time series. Note that since  $c_g = (\Omega/K) = \omega/(2k)$ ,  $\Omega$  being the modulation frequency and  $K$  the modulation wave number, the number of oscillations in a space series is half that in a time series  $N_x = (k/K) = \frac{1}{2}(\omega/\Omega) = \frac{1}{2}N_t$ . Furthermore, the surface elevation profile in a standing wave field is very sensitive to the measurement location.

Indeed, an excellent agreement can be noticed between laboratory experiments and numerical simulations, suggesting an elastic collision between the regular envelope and degenerate soliton [43] and by that confirming once again that the CNLSE framework may have an extended applicability range beyond the physical limitations technically limiting its exploitation.

Next, we extend our proof of concept validation study in considering a fully nonlinear water wave framework by numerically solving the Euler equations using the HOSM [46,47], which resolves up to 7-wave interactions in our simulations. This approach does not only allow for consideration of the wave evolution for a longer time and distance than at disposal in experimental wave facilities, but also provides a higher reliability compared with the

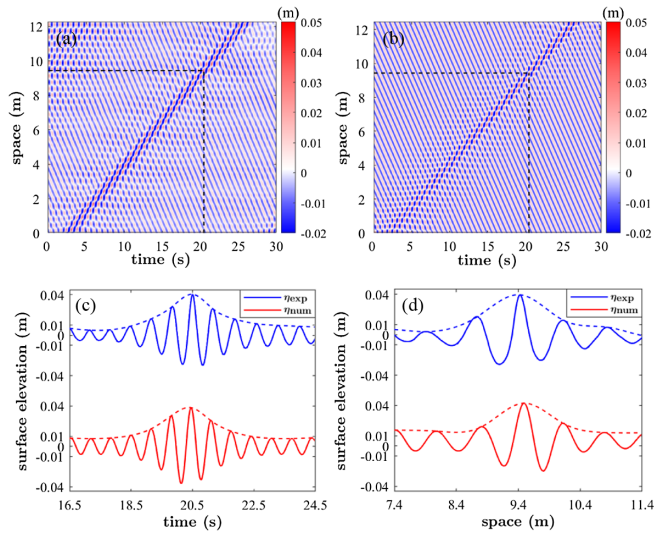


FIG. 4. (a) Evolution of a standing degenerate soliton for  $a = 0.01$  m and  $ak = 0.11$ . (b) Corresponding CNLSE simulations. (c) Comparison of the maximal temporal surface profile (top line) with the CNLSE prediction (bottom line). (d) Comparison of the maximal interpolated spatial surface profile (top line) with the CNLSE prediction (bottom line). The dashed line corresponds to the respective wave envelope profile, which has been extracted from the experimental data using the Hilbert transform.

weakly nonlinear CNLSE approach. Figure 5 shows a corresponding and particular case study, which has been experimentally studied and reported in Figs. 2(a) and 2(c), i.e., the case of the Peregrine breather on finite background. Because of the increase of the physical domain, the only difference is that the maximal wave focusing is expected to appear after 35 m of propagation while in the experiment only after 16 m. The initial condition at  $t = 0$  is specified in the form of two long trains with the carrier wave steepness  $ak = 0.09$  and amplitude  $a = 0.01$  m, and which travel toward each other. The rightward moving train is produced from the analytic PB solution; the inoculating perturbation is characterized by a steepness less than 0.11.

The pseudocolor in Fig. 5(a) represents the evolution of the surface displacement envelope, which is produced from two dozen simulations when various phase combinations were assigned to the initial wave trains. Hence, the envelope corresponds to the phase averaging of the upper enveloping surface. Only a part of the simulated domain is shown. The target focusing time according to the exact NLSE PB solution is about 90 wave periods; see the dashed black lines.

The snapshot of the maximum wave, which is very close to the breaking onset, is given by the black curve. Note that the deviations of the maximal envelope compression location are less significant in the wave flume because of the shorter propagating distance considered, a constraint imposed by the wave generator frequency range and the limited length of state of the art wave facilities.

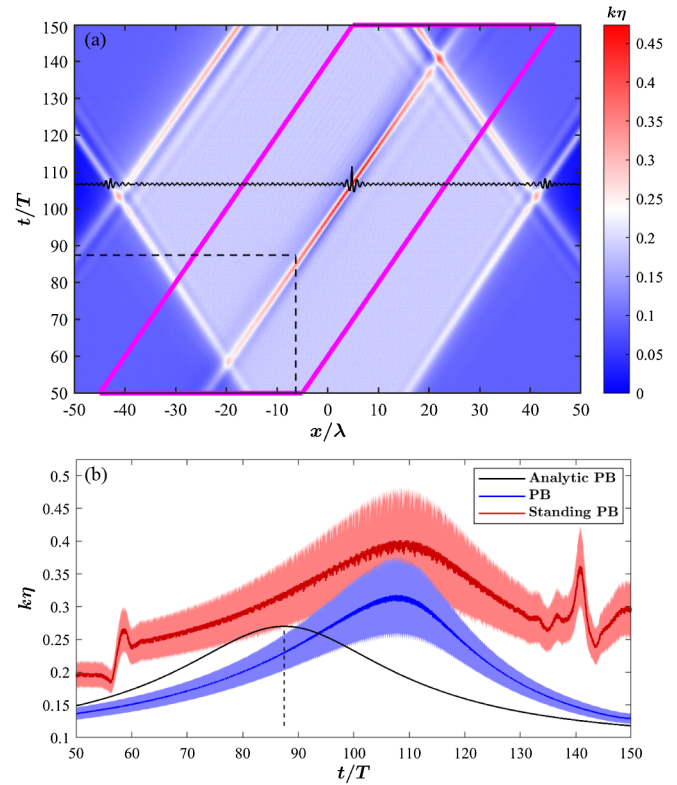


FIG. 5. Evolution of a PB in standing waves with the carrier steepness  $ak = 0.09$  as simulated by the HOSM by arranging two dozen phases allowing for the reconstruction of a wave envelope. (a) The surface displacement envelope  $k\eta$  is shown by the pseudocolor. The surface displacement profile of the highest focused wave is displayed in black while the dashed black lines point out the location of maximal envelope compression, both according to the analytic PB solution. The magenta parallelogram shows the area where the maximum wave amplitude is evaluated. The coordinate and time are normalized with the dominant wave length  $\lambda$  and period  $T$ , respectively. (b) Evolution of the maximum wave amplitude in the HOSM simulations and according to the analytic PB solution of the NLSE. The filled areas correspond to the intervals between crest and trough amplitudes, while the solid curves depict their simple means.

The strongly nonlinear simulations reproduce all the main features of the localized standing wave patterns as observed in the laboratory environment, particularly the clean and quasiundisturbed extreme wave focusing within the incident PB group. At the same time, the long evolution reveals some distinctions. In contrast to the weakly nonlinear framework, the strongly nonlinear simulation results, which include the physical effects of higher-order terms, correspond to slightly faster movement of the growing modulation and noticeably longer focusing time [48]. Besides, a minor asymmetry of the emerged large wave group is clearly seen before and after the maximal wave focusing.

The evolution of the corresponding maximum wave amplitude is displayed in Fig. 5(b) by the red color. It is

evaluated within the area bounded by the magenta contour in Fig. 5(a), which has been introduced to reduce the effect of emerging large modulations at the edges of the colliding wave trains. This dependence is compared with the result of similar strongly nonlinear numerical simulations of the PB when the opposite wave train is absent (blue color) and with the exact analytic PB solution (black curve). The differences between the red and blue curves correspond well to the amplitude of the opposite wave train at  $ak = 0.09$ , confirming once again the noninfluence of the oppositely propagating regular wave train on the focusing dynamics of the modulationally unstable wave packet. Considering the significantly longer fetch compared with the laboratory experiments, the strongly nonlinear localized focusing of Peregrine breathers on top of progressive or standing waves occurs later than predicted by CNLSE and results in significantly larger focused waves. This is a behavior which has been also quantified in the unidirectional NLSE case [48,49]. It is also interesting to note in Fig. 5(b) that the focusing delays seem to be the same for both the unidirectional (blue curves) and collinear case (red curves).

In conclusion, we have reported experimental evidence of quasiunperturbed PB hydrodynamics in standing waves. The same has been observed for the degenerate soliton, which is the counterpart of PB on zero background. Our results confirm that breather solutions of the NLSE can be considered to model and describe extreme wave localizations in nonintegrable systems [50,51]. Since experiments are always subject to dissipative effects, we believe that the role of NLSE solitons and breathers can be extended to a wider range of complex systems [52–54]. We also anticipate that our experimental work will motivate further studies to investigate the role of breathers for standing wave conditions in nonlinear dispersive media as well as to determine their function in crossing seas and vector nonlinear fiber-analog systems.

A. S. acknowledges the support from the RFBR Grant No. 21-55-15008 and from the Laboratory of Dynamical Systems and Applications NRU HSE (the Ministry of Science and Higher Education of the Russian Federation Grant No. 075-15-2019-1931). A. C. acknowledges support from Kyoto University's Hakubi Center for Advanced Research.

\*yuchen.he@sydney.edu.au

†chabchoub.amin.8w@kyoto-u.ac.jp

- [1] M. Onorato, S. Residori, U. Bortolozzo, A. Montina, and F. Arecchi, Rogue waves and their generating mechanisms in different physical contexts, *Phys. Rep.* **528**, 47 (2013).
- [2] J. M. Dudley, F. Dias, M. Erkintalo, and G. Genty, Instabilities, breathers and rogue waves in optics, *Nat. Photonics* **8**, 755 (2014).
- [3] P. Suret, A. Tikan, F. Bonnefoy, F. Copie, G. Ducrozet, A. Gelash, G. Prabhudesai, G. Michel, A. Cazaubiel, E. Falcon *et al.*, Nonlinear Spectral Synthesis of Soliton Gas in Deep-Water Surface Gravity Waves, *Phys. Rev. Lett.* **125**, 264101 (2020).
- [4] G. Vanderhaegen, C. Naveau, P. Szriftgiser, A. Kudlinski, M. Conforti, A. Mussot, M. Onorato, S. Trillo, A. Chabchoub, and N. Akhmediev, “Extraordinary” modulation instability in optics and hydrodynamics, *Proc. Natl. Acad. Sci. U.S.A.* **118**, e2019348118 (2021).
- [5] D. Weisman, C. M. Camesin, G. G. Rozenman, M. A. Efremov, L. Shemer, W. P. Schleich, and A. Arie, Diffractive Guiding of Waves by a Periodic Array of Slits, *Phys. Rev. Lett.* **127**, 014303 (2021).
- [6] V. E. Zakharov, Stability of periodic waves of finite amplitude on the surface of a deep fluid, *J. Appl. Mech. Tech. Phys.* **9**, 190 (1968).
- [7] F. Bonnefoy, F. Haudin, G. Michel, B. Semin, T. Humbert, S. Aumaître, M. Berhanu, and E. Falcon, Observation of resonant interactions among surface gravity waves, *J. Fluid Mech.* **805**, R3 (2016).
- [8] M. Longuet-Higgins, Breaking waves in deep or shallow water, in *Proceedings of the 10th Conference on Naval Hydrodynamics* (MIT, Cambridge, MA, 1974), Vol. 597, p. 605.
- [9] M. L. McAllister, S. Draycott, T. Adcock, P. Taylor, and T. Van Den Bremer, Laboratory recreation of the draupner wave and the role of breaking in crossing seas, *J. Fluid Mech.* **860**, 767 (2019).
- [10] J. M. Dudley, G. Genty, A. Mussot, A. Chabchoub, and F. Dias, Rogue waves and analogies in optics and oceanography, *Nat. Rev. Phys.* **1**, 675 (2019).
- [11] T. Waseda, Nonlinear processes, in *Ocean Wave Dynamics* (World Scientific, 2020), pp. 103–161.
- [12] V. Bespalov and V. Talanov, Filamentary structure of light beams in nonlinear liquids, *Sov. J. Exp. Theor. Phys. Lett.* **3**, 471 (1966), [http://jetpletters.ru/ps/1621/article\\_24803.shtml](http://jetpletters.ru/ps/1621/article_24803.shtml).
- [13] T. B. Benjamin and J. E. Feir, The disintegration of wave trains on deep water part 1. Theory, *J. Fluid Mech.* **27**, 417 (1967).
- [14] T. Waseda, T. Kinoshita, and H. Tamura, Evolution of a random directional wave and freak wave occurrence, *J. Phys. Oceanogr.* **39**, 621 (2009).
- [15] M. Onorato, D. Proment, and A. Toffoli, Freak waves in crossing seas, *Eur. Phys. J. Spec. Top.* **185**, 45 (2010).
- [16] O. Gramstad, E. Bitner-Gregersen, K. Trulsen, and J. C. Nieto Borge, Modulational instability and rogue waves in crossing sea states, *J. Phys. Oceanogr.* **48**, 1317 (2018).
- [17] P. A. Janssen, Nonlinear four-wave interactions and freak waves, *J. Phys. Oceanogr.* **33**, 863 (2003).
- [18] N. Mori, M. Onorato, and P. A. Janssen, On the estimation of the kurtosis in directional sea states for freak wave forecasting, *J. Phys. Oceanogr.* **41**, 1484 (2011).
- [19] A. Grönlund, B. Eliasson, and M. Marklund, Evolution of rogue waves in interacting wave systems, *Europhys. Lett.* **86**, 24001 (2009).
- [20] M. Okamura, Instabilities of weakly nonlinear standing gravity waves, *J. Phys. Soc. Jpn.* **53**, 3788 (1984).
- [21] M. Onorato, A. R. Osborne, and M. Serio, Modulational Instability in Crossing Sea States: A Possible Mechanism for the Formation of Freak Waves, *Phys. Rev. Lett.* **96**, 014503 (2006).

- [22] F. Baronio, A. Degasperis, M. Conforti, and S. Wabnitz, Solutions of the Vector Nonlinear Schrödinger Equations: Evidence for Deterministic Rogue Waves, *Phys. Rev. Lett.* **109**, 044102 (2012).
- [23] B. Frisquet, B. Kibler, P. Morin, F. Baronio, M. Conforti, G. Millot, and S. Wabnitz, Optical dark rogue wave, *Sci. Rep.* **6**, 20785 (2016).
- [24] S. Støle-Hentschel, K. Trulsen, L. B. Rye, and A. Raustøl, Extreme wave statistics of counter-propagating, irregular, long-crested sea states, *Phys. Fluids* **30**, 067102 (2018).
- [25] J. N. Steer, M. L. McAllister, A. G. Borthwick, and T. S. Van Den Bremer, Experimental observation of modulational instability in crossing surface gravity wavetrains, *Fluids* **4**, 105 (2019).
- [26] D. H. Peregrine, Water waves, nonlinear Schrödinger equations and their solutions, *J. Aust. Math. Soc. Series B, Appl. Math.* **25**, 16 (1983).
- [27] O. Gramstad and K. Trulsen, Fourth-order coupled nonlinear Schrödinger equations for gravity waves on deep water, *Phys. Fluids* **23**, 062102 (2011).
- [28] B. Kibler, J. Fatome, C. Finot, G. Millot, F. Dias, G. Genty, N. Akhmediev, and J. M. Dudley, The Peregrine soliton in nonlinear fibre optics, *Nat. Phys.* **6**, 790 (2010).
- [29] A. Chabchoub, N. P. Hoffmann, and N. Akhmediev, Rogue Wave Observation in a Water Wave Tank, *Phys. Rev. Lett.* **106**, 204502 (2011).
- [30] H. Bailung, S. K. Sharma, and Y. Nakamura, Observation of Peregrine Solitons in a Multicomponent Plasma with Negative Ions, *Phys. Rev. Lett.* **107**, 255005 (2011).
- [31] N. N. Akhmediev and A. Ankiewicz, *Solitons: Nonlinear Pulses and Beams* (Chapman & Hall, London, 1997).
- [32] A. Osborne, *Nonlinear Ocean Waves and the Inverse Scattering Transform* (Academic Press, New York, 2010).
- [33] N. Akhmediev, V. Eleonskii, and N. Kulagin, Generation of periodic trains of picosecond pulses in an optical fiber: Exact solutions, *Sov. Phys. JETP* **62**, 894 (1985), <http://jetp.ras.ru/cgi-bin/r/index/e/62/5/p894?a=list>.
- [34] L. Cavaleri, L. Bertotti, L. Torrisi, E. Bitner-Gregersen, M. Serio, and M. Onorato, Rogue waves in crossing seas: The Louis majesty accident, *J. Geophys. Res.* **117** (2012).
- [35] E. A. Kuznetsov, Solitons in a parametrically unstable plasma, *Sov. Phys. Dokl.* **22**, 507 (1977).
- [36] A. Chabchoub, A. Slunyaev, N. Hoffmann, F. Dias, B. Kibler, G. Genty, J. M. Dudley, and N. Akhmediev, The Peregrine breather on the zero-background limit as the two-soliton degenerate solution: An experimental study, *Front. Phys.* **9**, 633549 (2021).
- [37] M. Tanter, J.-L. Thomas, and M. Fink, Influence of boundary conditions on time-reversal focusing through heterogeneous media, *Appl. Phys. Lett.* **72**, 2511 (1998).
- [38] A. Chabchoub and R. H. Grimshaw, The hydrodynamic nonlinear Schrödinger equation: Space and time, *Fluids* **1**, 23 (2016).
- [39] Y. He, A. Slunyaev, N. Mori, and A. Chabchoub, See Supplemental Material at <http://link.aps.org/supplemental/10.1103/PhysRevLett.129.144502> for video showing the formation of standing waves and the unperturbed wave focusing of the Peregrine breather in the wave tank.
- [40] Y. Goda and Y. Suzuki, Estimation of incident and reflected waves in random wave experiments, in *Coastal Engineering 1976* (ASCE Library, 1977), pp. 828–845.
- [41] P. J. Aguilera-Rojas, M. G. Clerc, G. Gonzalez-Cortes, and G. Jara-Schulz, Localized standing waves induced by spatiotemporal forcing, *Phys. Rev. E* **104**, 044209 (2021).
- [42] A. Dyachenko, D. Kachulin, and V. Zakharov, Super compact equation for water waves, *J. Fluid Mech.* **828**, 661 (2017).
- [43] A. Dyachenko, Canonical system of equations for 1D water waves, *Stud. Appl. Math.* **144**, 493 (2020).
- [44] A. V. Slunyaev, Group-wave resonances in nonlinear dispersive media: The case of gravity water waves, *Phys. Rev. E* **97**, 010202(R) (2018).
- [45] D. Kedziora, A. Ankiewicz, and N. Akhmediev, Rogue waves and solitons on a cnoidal background, *Eur. Phys. J. Spec. Top.* **223**, 43 (2014).
- [46] B. West, K. Brueckner, R. Janda, D. Milder, and R. Milton, A new numerical method for surface hydrodynamics, *J. Geophys. Res.* **92**, 11803 (1987).
- [47] D. G. Dommermuth and D. K. Yue, A high-order spectral method for the study of nonlinear gravity waves, *J. Fluid Mech.* **184**, 267 (1987).
- [48] A. Slunyaev, E. Pelinovsky, A. Sergeeva, A. Chabchoub, N. Hoffmann, M. Onorato, and N. Akhmediev, Super-rogue waves in simulations based on weakly nonlinear and fully nonlinear hydrodynamic equations, *Phys. Rev. E* **88**, 012909 (2013).
- [49] L. Shemer and L. Alperovich, Peregrine breather revisited, *Phys. Fluids* **25**, 051701 (2013).
- [50] Y. S. Kivshar and B. A. Malomed, Dynamics of solitons in nearly integrable systems, *Rev. Mod. Phys.* **61**, 763 (1989).
- [51] I. S. Chekhovskoy, O. V. Shtyrina, M. P. Fedoruk, S. B. Medvedev, and S. K. Turitsyn, Nonlinear Fourier Transform for Analysis of Coherent Structures in Dissipative Systems, *Phys. Rev. Lett.* **122**, 153901 (2019).
- [52] M. Haelterman, S. Trillo, and S. Wabnitz, Dissipative modulation instability in a nonlinear dispersive ring cavity, *Opt. Commun.* **91**, 401 (1992).
- [53] N. Akhmediev and A. Ankiewicz, *Dissipative Solitons: From Optics to Biology and Medicine* (Springer Science & Business Media, New York, 2008), Vol. 751.
- [54] A. U. Nielsen, Y. Xu, C. Todd, M. Ferré, M. G. Clerc, S. Coen, S. G. Murdoch, and M. Erkintalo, Nonlinear Localization of Dissipative Modulation Instability, *Phys. Rev. Lett.* **127**, 123901 (2021).